Wind and Structures, *Vol. 31, No. 1 (2020) 59-73*
DOI: https://doi.org/10.12989/was.2020.31.1.59

Wind fragility analysis of RC chimney with temperature effects by dual response surface method

Gaurav Datta[a], Avinandan Sahoo[b] and Soumya Bhattacharjya*

Department of Civil Engineering, Indian Institute of Engineering Science and Technology (IIEST), Shibpur, Howrah.-711103. West Bengal, India

(*Received October 31, 2019, Revised April 17, 2020, Accepted June 11, 2020*)

Abstract. Wind fragility analysis (WFA) of concrete chimney is often executed disregarding temperature effects. But combined wind and temperature effect is the most critical limit state to define the safety of a chimney. Hence, in this study, WFA of a 70 m tall RC chimney for combined wind and temperature effects is explored. The wind force time-history is generated by spectral representation method. The safety of chimney is assessed considering limit states of stress failure in concrete and steel. A moving-least-squares method based dual response surface method (DRSM) procedure is proposed in WFA to alleviate huge computational time requirement by the conventional direct Monte Carlo simulation (MCS) approach. The DRSM captures the record-to-record variation of wind force time-histories and uncertainty in system parameters. The proposed DRSM approach yields fragility curves which are in close conformity with the most accurate direct MCS approach within substantially less computational time. In this regard, the error by the single-level RSM and least-squares method based DRSM can be easily noted. The WFA results indicate that over temperature difference of 150°C, the temperature stress is so pronounced that the probability of failure is very high even at 30 m/s wind speed. However, below 100°C, wind governs the design.

Keywords: fragility; wind force; temperature; RC chimney; Monte Carlo simulation; dual response surface method

1. Introduction

The state-of-the-art of deterministic wind design of tall reinforced concrete (RC) chimney is quite advanced. Apart from Indian Standard (IS) code (IS 4998-I 2015), there have been notable researches focusing best possible shape of chimney (Park *et al.* 2016), wind effect on chimney (Karaca and Turkeli 2014, Liang *et al.* 2018), seismic retrofitting (Bru *et al.* 2017) and condition assessment by modal testing (Sancibrian *et al.* 2017). These researches are mostly in the deterministic domain, i.e. assuming all the involved parameters and load effects are at fixed values. However, it is well established now that such deterministic safety assessments disregarding the uncertainty effect may invite catastrophic consequences (Venanzi *et al.* 2015). The uncertain parameters will vary randomly instead of staying at their pre-assumed fixed values. As a result, the limit state functions will also vary randomly. Such variation of limit state may lead to even practically unsafe situation, though the design is apparently safe in the deterministic domain. In this regard, the influence of parameter uncertainty on chimney has been studied by Kareem (1988). Reliability assessment of RC chimney was presented by First Order Second Moment method in Kareem and Hseih (1986) and by Monte Carlo simulation (MCS) in Kareem (1990).

The MCS based approach is particularly suitable for higher levels of uncertainty. The safety of a structure subjected to uncertain wind loading can be best assessed by a fragility analysis. Fragility is the probability that a response quantity of both structural and non-structural system exceeds a critical threshold if subjected to dynamic loading of specified intensity. In fact, there have been plenty of researches on wind fragility analysis (WFA) of structures like buildings (Smith and Caracoglia 2011, Bhandari *et al.* 2018), container cranes (Gur and Ray-Chaudhuri 2014), wood-frame structures (Lee and Rosowsky 2006), and towers (Giaccu and Caracoglia 2018). The WFA of urban trees in high wind areas of Southeast China (Peng *et al.* 2018a) is also of worth mentioning here. However, WFA of chimney has been a comparatively less explored field, though seismic fragility assessment of tall chimneys is comparatively well explored (Zhou *et al.* 2015, Zhou *et al.* 2017).

In recent years, WFA of chimney was accomplished in the frequency domain by Ambrosini *et al.* (2002). However, the authors disregarded temperature effects in assessing the safety of the chimney. Moreover, for chimney-like structure, the temperature effect is indispensable and is most likely that high-temperature difference may prevail in the chimney when a storm strike. That is why the present standards (IS:456 2000, IS:4998-I 2015) consider the combined effect of wind temperature as a 'must check' limit state of failure. Thus, WFA remains incomplete unless the combined limit states of wind and temperature are considered. In fact, this limit states generally governs the design of RC chimney (Bhavikatti 2014). The present study investigates WFA of chimney considering temperature effects, where uncertainty

*Corresponding author, Ph.D. Associate Professor
E-mail: soumyaiiests@gmail.com
[a]Research Scholar
[b]Post Graduate Scholar

http://www.techno-press.com/journals/was&subpage=7 ISSN: 1226-6116 (Print), 1598-6225 (Online)

in both wind and temperature has been incorporated. Since the WFA of RC chimney including temperature effect is observed to be scarce in the existing literature; it constitutes the uniqueness of the present study.

Conventionally, the dynamic analysis of structures under wind excitation is carried out as an equivalent static wind load analysis by means of the gust factor method (Chen and Kareem 2004). However, during extreme wind events, there is a high chance of temporal wind speed fluctuation and spatial variation in the wind field. This approach is incapable to capture the influence of spatially varying wind field on the response of structures such as large chimneys. Thus, to investigate the effect of spatially varying wind field on structures, time-history analysis is necessary for accurate quantification of response (Deodatis and Micaletti 2001, Martinez-Vazquez 2016, Zeng *et al.* 2017). It is now understood that the traditional deterministic method of wind-resistant design cannot ensure the expected performance level and guarantee the safety of structure (Chen *et al.* 2017). Thus, probabilistic quantification of wind-induced vibration and reliability-based wind-resistant design are indeed required in practice for wind-sensitive structures.

The wind effect is simulated in this paper by generating artificial wind field using weighted amplitude wave superposition technique. In this regard, Kaimal's power spectral density function (PSDF) (Kaimal *et al.* 1972) is used. Effect of coherence is also taken into account following Li *et al.* (2004). This approach of artificial wind force generation has been successfully used in WFA of structures (Gur and Ray-Chaudhuri 2014, Bhandari *et al.* 2018). Other ways of obtaining wind force distribution over height, space and time are by wind tunnel experiments or by computational fluid dynamics. However, these approaches will require execution of a large number of experimentations (or computer simulations) and thus result in exorbitantly high simulation time to generate the random wind field. Hence, in the present study, the random wind field is simulated by generating artificial wind force time-histories considering uncertainty in the related parameters. The record-to-record variation of random wind speed for the same wind hazard data is captured by applying dual response surface method (DRSM). Once the artificial wind force time-histories are generated, the response of RC chimney is easily obtained by performing linear time-history analyses of finite element model of the chimney. The temperature effect is combined with the most critical wind response values.

It may be noted here that the response of the structure is implicit with respect to input parameters. Thereby, execution of the WFA by conventional direct MCS framework would involve an exorbitantly large number of finite element analyses (FEA). To obtain one point on the fragility analysis by the direct MCS, one needs to execute the simulation until the MCS converges. Say, the MCS converges at 1,000 simulations. This means the FEA of the chimney has to be repeated for 1,000 times. Now, for one complete response evaluation of the RC chimney (starting from wind force generation to the completion of linear time-history analysis) the time requirement is generally around 15 minutes with 8GB RAM and 3.7 GHz processor unit. Hence, the time required for obtaining a single point in the fragility curve will be $1{,}000\times 15=15{,}000$ minutes, i.e. 416 hours. Now, to obtain a complete fragility curve at different wind speed intensities, this process has to be repeated for multiple times. Thus, the WFA in the direct MCS framework is a computationally exhaustive approach and there must be some tricks to alleviate this onerous computational time requirement.

This issue of extensive computational time required for the WFA by the direct MCS is tackled in the present paper by proposing a DRSM based WFA formulation. In recent years, a trend has been observed in seismic fragility analysis of structure to apply the single level RSM (Bhattacharjya and Chakraborty 2018, Feng *et al.* 2018) or the DRSM (Ghosh *et al.* 2017a, Ghosh *et al.* 2017b) within the MCS framework which decouples FEA and response analysis modules from the main simulation loop. In the single level RSM based approach, one response equation for limit state function is generated as a function of input parameters. Then, the MCS is adopted to incorporate uncertainty in the input parameters. The single-level RSM may not be adequate for WFA of RC chimney in the time domain due to the random nature of wind. In fact, the artificially generated wind force time-history will vary even for the same set up of wind speed, wind incidence angle and other system parameters. This aspect of record-to-record variation of wind force time-history cannot be considered using single-level RSM (Bhandari *et al.* 2018). On the other hand, in the DRSM, for the same set up of input parameters, a number of wind speed time-histories are generated. Thus, at each design of experiment (DOE) point, two response surfaces are formed, one for mean response and another for the standard deviation (SD) of the response. The number of FEA runs will obviously increase by the DRSM compared to single-level RSM. However, the computational time by the DRSM is an order lesser than the direct MCS approach. Moreover, the application of single-level RSM in WFA may be erroneous as it does not consider the record-to-record variation of wind speed time-histories. It is of worth mentioning at this point that the application of DRSM is not yet investigated in WFA and hence builds another uniqueness of the study. It may be further noted that by the proposed DRSM based WFA approach, the MCS is no longer needed to be performed once the two response surface equations are developed by the DRSM. Thus, a substantial amount of computational time is saved by the proposed approach.

2. Wind fragility analysis

The structural safety under random load is generally evaluated in terms of fragility, i.e. the probability of exceeding allowable response level of structure for a specified intensity of wind load. Using the wind hazard, wind incident angle and dynamic response statistics, the risk of a structure under stochastic wind load is obtained as:

$$P_f = \int_{\phi=0}^{2\pi} \int_{v=0}^{v_{max}} \left\{ P\left[\left(y > y_a \right)\Big|_{v,\phi} \right] \right\} f\left(v,\phi\right) dv d\phi \qquad (1)$$

where, $P\left[\left(y > y_a\right)\big|_{v,\phi}\right]$ is referred as fragility, $F_r(v,\phi)$, which is the focus of the present study. The fragility is the probability that the response 'y' will exceed the allowable threshold response y_a when subjected to the wind of speed v attacking at an angle, ϕ. In Eq. (1), v_{max} is the maximum value of wind speed considered in the analysis. $f(v,\phi)$ is the joint probability density function (PDF) of the maximum wind speed (i.e., wind hazard). For axis symmetrical problem like chimney, fragility is invariant of ϕ and thus Eq. (1) can be re-written as:

$$\begin{aligned} P_f &= \int_{v=0}^{v_{max}} \left\{P\left[\left(y > y_a\right)\big|_v\right]\right\} f(v)\,dv \\ &= \int_{v=0}^{v_{max}} F_r(v)\, f(v)\,dv \end{aligned} \tag{2}$$

In the present paper, maximum stresses in concrete and steel under combined wind and temperature effects are considered as the response quantities, which are obtained by FEA of chimney. Let, $\Upsilon(\mathbf{\Theta})$ denotes the RSM yielded explicit functional form of critical limit state 'y' resulting out of the response quantities and $\mathbf{\Theta}$ represents a vector of random parameters (which are the regressors of RSM). The MCS is applied over $\Upsilon(\mathbf{\Theta})$. If the MCS converges at N number of simulations and n_f is the number of simulations for which $\{y = \Upsilon(\mathbf{\Theta})\} > y_a$, the fragility of Eq. (2) can be expressed as:

$$F_r(v) = P\left[\left(\{y = \Upsilon(\mathbf{\Theta})\} > y_a\right)\big|_v\right] = \left(n_f / N\right) \tag{3}$$

Since the effect of temperature difference ΔT also acts as another hazard, the above equation is re-written as:

$$F_r(v,\Delta T) = P\left[\left(\{y = \Upsilon(\mathbf{\Theta})\} > y_a\right)\big|_{v,\,\Delta T}\right] = \left(n_f^{'} / N\right) \tag{4}$$

In the above, $n_f^{'}$ is the number of simulations for which the limit state is violated. The relationship between y and uncertain parameters, $\mathbf{\Theta}$ is implicit. As already discussed, the DRSM is used in the present paper to obtain an explicit functional relationship between y and $\mathbf{\Theta}$. This is presented in the next section.

3. The dual RSM

The input variable space is usually separated into two groups by the DRSM, viz. i) the structural parameters and ii) the stochastic sequences. Stochasticity due to the wind is implicitly incorporated in the analysis by using a suite of wind force time-histories to consider the record-to-record variations. In the DRSM, at first for each DOE point (each DOE point corresponds to a particular v), a number of wind speed time-histories are generated. The mean and SD of response are obtained for each DOE point. This is repeated for all DOE points (which includes a set of different v). In this way, two vectors, viz. a mean vector $\mathbf{y}_\mu$ and a SD vector, $\mathbf{y}_\sigma$ of the desired responses `$\mathbf{y}$` are generated. Then the response surface for mean and SD are obtained for the considered responses i.e.

$$y_\mu = g(\mathbf{\Theta}) \quad \text{and} \quad y_\sigma = h(\mathbf{\Theta}) \tag{5}$$

A goodness of fit test is conducted to ascertain the distribution of 'y' based on the available DOE data. If 'y' is observed to follow extreme value type I distribution, the cumulative distribution function (CDF) of y is given as:

$$F_Y(y) = exp\left[-exp\left\{-\alpha_n\left(y_a - u_n\right)\right\}\right] \tag{6}$$

with, $\alpha_n = 1/\sqrt{6}\left(\pi/y_\sigma\right)$ and $u_n = y_\mu - 0.5772/\alpha_n$.

Thus, the fragility function of Eq. (3) can now be expressed as:

$$F_r(v) = P(y > y_a) = 1 - P(y < y_a) = 1 - F_Y(y_a) \tag{7a}$$

Using Eqns. (5) - (6), Eq. (7a) can be re-written as:

$$F_r(v) = 1 - exp\left[-exp\left\{\begin{array}{l} -\dfrac{1}{\sqrt{6}}\left(\dfrac{\pi}{h(\mathbf{\Theta})}\right)\times \\ \left(y_a - g(\mathbf{\Theta}) + \dfrac{0.5772}{\left(\dfrac{1}{\sqrt{6}}\left(\dfrac{\pi}{h(\mathbf{\Theta})}\right)\right)}\right)\end{array}\right\}\right] \tag{7b}$$

Thus, the fragility is a direct function of the two response surfaces $g(\mathbf{\Theta})$ and $h(\mathbf{\Theta})$. Once $g(\mathbf{\Theta})$ and $h(\mathbf{\Theta})$ are obtained, the MCS is no longer required to calculate fragility. In this way, substantial computational time can be saved in the WFA by the proposed approach with respect to the conventional MCS based approach. Generally, the RSM expressions are obtained by conventional least-squares method (LSM). However, recent researches (Zhao *et al.* 2017, Bhattacharjya *et al.* 2019) indicate the possibility of error inclusion by the LSM. Thus, in the present paper, a more efficient moving-least-squares method (MLSM) has been adopted in the DRSM.

4. The MLSM based DRSM

The dynamic response quantity of the structure $y = \Upsilon(\mathbf{\Theta})$ is generally approximated by the LSM based RSM. Consider, $\Re$ response values $y_\Re$, corresponding to $\Re$ numbers of observed input data Θ_{ij} (which denotes the i^{th} observation of the regressor Θ_j in the DOE). The relationship between the predicted response, $\hat{y}$ and the regressor variables, $\mathbf{\Theta}$ is expressed by the polynomial RSM as (Myers *et al.* 2016):

$$\hat{y} = \Upsilon(\mathbf{\Theta}) = \beta_0 + \sum_{i=1}^{n} \beta_i \Theta_i + \sum_{i=1}^{n} \beta_{ii} \Theta_i^2 + \sum_{i<j=2}^{n} \beta_{ij} \Theta_i \Theta_j \quad (8)$$

where, n is the number of regressors. Now, after assembling all the points in dataset, the above relationship can be cast in the matrix form as $\hat{\mathbf{y}} = \mathbf{Q}\boldsymbol{\beta}$, where, $\mathbf{Q}$ and $\boldsymbol{\beta}$ are the design matrix (which contains the input data from the DOE), and the unknown co-efficient vector, respectively. Then, the relationship between the actual response vector $\mathbf{y}$ and the predicted response $\hat{\mathbf{y}}$ can be expressed as:

$$\mathbf{y} = \hat{\mathbf{y}} + \boldsymbol{\xi} = \mathbf{Q}\boldsymbol{\beta} + \boldsymbol{\xi} \quad (9)$$

In the above, $\boldsymbol{\xi}$ is the error vector. The unknown polynomial coefficient vector is obtained by minimizing an error norm which represents the sum of the squares of errors as:

$$\begin{aligned} Err_y &= \sum_{i=1}^{\Re} \left(y_i - \sum_{i=1}^{n} \beta_i \Theta_i - \sum_{i=1}^{n} \beta_{ii} \Theta_i^2 - \sum_{i<j=2}^{n} \beta_{ij} \Theta_i \Theta_j \right)^2 \\ &= (\mathbf{y} - \hat{\mathbf{y}})^{\mathrm{T}} (\mathbf{y} - \hat{\mathbf{y}}) = \left(\mathbf{y} - \mathbf{Q}^*\boldsymbol{\beta}\right)^{\mathrm{T}} \left(\mathbf{y} - \mathbf{Q}^*\boldsymbol{\beta}\right) \end{aligned} \quad (10)$$

in which, $\mathbf{Q}^*$ is the design matrix whose elements are evaluated at the DOE points. Minimizing error norm yields:

$$\boldsymbol{\beta} = \left[\mathbf{Q}^{*\mathrm{T}} \mathbf{Q}^*\right]^{-1} \mathbf{Q}^{*\mathrm{T}} \mathbf{y} \quad (11)$$

It can be noted from above that the coefficient vector by the LSM remains invariant over the whole domain of interpretation. In other words, the LSM yields a global fit. As a result, the problem of under-fitting may arise for the LSM, yielding large approximating errors. In this regard, the MLSM based RSM predicts a local approximation of the scatter data based on the point of interest (prediction point). The MLSM based RSM is a weighted LSM that has varying weight functions with respect to the position of approximation. The weight associated with a particular sampling point $\mathbf{\Theta}_i$ decays as the prediction point $\mathbf{\Theta}$ moves away from $\mathbf{\Theta}_i$. The weight function is defined around $\mathbf{\Theta}$ and its magnitude changes with $\mathbf{\Theta}$. The MLSM captures localized variations of the response by virtue of this weight function and significantly reduces the curse of underfitting. The modified error norm $Err_y(\mathbf{\Theta})$ can be defined as the sum of the weighted errors as:

$$Err_y(\mathbf{\Theta}) = \xi^{\mathrm{T}} \mathbf{W}(\mathbf{\Theta}) \xi = (\mathbf{y} - \hat{\mathbf{y}})^{\mathrm{T}} \mathbf{W}(\mathbf{\Theta}) (\mathbf{y} - \hat{\mathbf{y}}) = \left(\mathbf{y} - \mathbf{Q}^*\boldsymbol{\beta}\right)^{\mathrm{T}} \mathbf{W}(\mathbf{\Theta}) \left(\mathbf{y} - \mathbf{Q}^*\boldsymbol{\beta}\right) \quad (12)$$

Here, $\mathbf{W}(\mathbf{\Theta})$ is the diagonal matrix of the weight function and it depends on the location of $\mathbf{\Theta}$. $\mathbf{W}(\mathbf{\Theta})$ is obtained by utilizing a weighting function as (Taflanidis and Cheung 2012):

$$w(\mathbf{\Theta} - \mathbf{\Theta}_i) = w(\mathbf{d}_i) = \left(e^{-\left(\frac{\|\mathbf{d}_i\|}{c\Gamma}\right)^{2\lambda}} - e^{-\left(\frac{1}{c}\right)^{2\lambda}} \right) \Bigg/ \left(1 - e^{-\left(\frac{1}{c}\right)^{2\lambda}} \right), \quad (13)$$

$$\text{if } \|\mathbf{d}_i\| < \Gamma \text{ ; else, } w(\mathbf{d}_i) = 0$$

where, Γ is the diameter of the sphere of influence around $\mathbf{\Theta}_i$, which is chosen to cover a sufficient number of neighbouring points evading the under-fitting problem. In the present study, Γ is chosen as twice the distance between the most extreme experimental point out of $(1+2n)^{\text{th}}$ scatter data points (Goswami *et al.* 2016). $\|\mathbf{d}_i\|$ is the Euclidean distance between the sampling point, $\mathbf{\Theta}_i$, and the prediction point, $\mathbf{\Theta}$; and c, λ are the free parameters to be selected for better efficiency. It is of worth mentioning here that there is a chance of overfitting by both the LSM and the MLSM. In such a case, the response surface model captures the noise or random fluctuations in the training data. As a result, because of the captured noise, the developed response surface model may fail to accurately predict the response for new datasets. Now, for the LSM, there is no regulating parameter restricting the overfitting problem. However, for the MLSM, the parameter c serves to take care of this aspect. When a higher value (>1.0) of c is chosen, the MLSM approaches towards a conventional LSM based RSM, i.e., the local approximation is no longer working. On the other hand, if a very low value (<0.1) is taken for c, then very few DOE points closer to the prediction point get hugely weighted compared to the other DOE points, resulting in overfitting. Hence, the selection of a value for c should be a balance between a local approximation and accuracy by avoiding near-singular problem. It has been already reported in the existing literature that if the parameters 'c' and 'λ' take the values 0.4 and 1.0, respectively, both the problems of under-fitting and overfitting can be alleviated (Taflanidis and Cheung 2012, Bhandari *et al.* 2018, Ghosh *et al.* 2018). Moreover, in the present study, the accuracy of the generated response surface is cross-validated by taking new test points which are not used to construct the response surface. If the validation is unsuccessful a fresh DOE is generally taken to re-construct the response surface. In this regard, one can refer re-sampling techniques like k-fold cross-validation approach (Reuter *et al.* 2017).

The weight matrix $\mathbf{W}(\mathbf{\Theta})$ can be constructed by using the weighting functions in diagonal terms as:

$$\mathbf{W}(\mathbf{\Theta}) = \begin{bmatrix} w(\mathbf{\Theta} - \mathbf{\Theta}_1) & 0 & \cdots & 0 \\ 0 & w(\mathbf{\Theta} - \mathbf{\Theta}_2) & \cdots & 0 \\ \cdots & \cdots & \cdots & \cdots \\ 0 & 0 & \cdots & w(\mathbf{\Theta} - \mathbf{\Theta}_n) \end{bmatrix} \quad (14)$$

The least-squares estimate of $\boldsymbol{\beta}$ is then obtained as (Myers *et al.* 2016):

$$\boldsymbol{\beta} = \left[\mathbf{Q}^{*T}\mathbf{W}(\boldsymbol{\Theta})\mathbf{Q}^{*}\right]^{-1}\mathbf{Q}^{*T}\mathbf{W}(\boldsymbol{\Theta})\mathbf{y} \tag{15}$$

Once $\boldsymbol{\beta}$ is evaluated by the above equation, the response: $\hat{y} = \Upsilon(\boldsymbol{\Theta})$ can be readily evaluated for any set of input parameters, $\boldsymbol{\Theta}$.

In the present paper, the MLSM based DRSM is used to execute WFA. However, for the sake of comparison, the analysis has been also done by the most accurate direct MCS approach and the conventional LSM based DRSM.

5. Generation of wind force time-history

In the present study, the random wind field has been simulated by generating artificial wind force time-histories through spectral representation method (SRM). Due to its accuracy and simplicity, the SRM is a widely used method in the simulation of stochastic processes and random fields (Shinozuka 1971, Di Paola 1998, Benowitz and Deodatis 2015, Liu *et al.* 2018). In fact, this spectral representation is derived based on real data. The stochastic wind field model presented in this paper is well accepted and has been already used in Gur and Ray-Chaudhuri (2014), Bhandari *et al.* (2018) and Chen *et al.* (2019).

In general, the along-wind component of wind force acting at i^{th} level at height z from the ground can be written as:

$$F_D(z,t) = \frac{1}{2}\rho\left[V(z,t)\right]^2 C_D A_i \tag{16}$$

In above, the wind speed, $V(z,t)$, is composed of time-invariant mean component $\bar{V}(z)$, and a fluctuating component $v(t)$, known as gust; i.e. $V(z,t) = \bar{V}(z) + v(t)$. The mean wind speed profile $\bar{V}(z)$ is expressed by a power law (Simiu and Scanlan 1986) as: $\bar{V}(z) = V_G\left(z/z_G\right)^{1/\zeta}$, where, V_G is the gradient wind speed, z_G is the gradient height, and ζ is an exponent. The values of z_G and ζ depend on ground surface roughness. In the numerical study, z_G =12.5 m and ζ =7 have been considered following Chen and Letchford (2004). C_D is the drag coefficient, which is invariant over height. In the present study, the value of C_D is obtained from IS 875(III) (2015) since the structure considered is regular in shape and size. However, for irregular structures, C_D may be estimated from a wind tunnel test or by computational fluid dynamic analysis.

The gust component $v(t)$ is a major source of randomness. Most commonly, the random nature of the gust is modelled by its PSDF. In this study, the gust component is generated by using Kaimal's PSDF which can be expressed as:

$$S_u(\Omega,z) = 50u_*^2 z \Big/ \left\{\pi\bar{V}(z)\left[1+50\left(|\Omega|\, z/2\pi\bar{V}(z)\right)\right]^{5/3}\right\} \tag{17}$$

where, $\Omega(=2\pi f)$ is the frequency in rad/s, and f is in Hz. The shear velocity u_* is computed by logarithmic law of mean velocity as (Ambrosini *et al.* 2002), $u_* = \kappa\bar{V}/ln(z/z_0)$, in which, κ is the von Karman constant, taken as 0.4 (Tabbuso *et al.* 2016), and z_0 is the roughness length of the surface which depends on the surface properties only and can be taken as 0.01 for smooth surface (Chen and Letchford 2004). It may be noted here that the wind directionality with respect to the orientation of a structure and coherence seem to have substantial effects on wind response (Abrous *et al.* 2015, Benowitz and Deodatis 2015). Thus, in the present study, a more realistic wind field model accounting wind directionality and coherence is taken up. In natural wind fields, the wind speed and phase of the calculated points at different heights are different due to the turbulence. The associated correlation is generally expressed as a coherence function. The along-wind coherence $\eta_{jk}(\Omega,dx)$ and across-wind coherence $\gamma_{jk}(\Omega,dy,dz)$ can be estimated as (Harris 1990, Ambrosini *et al.* 2002):

$$\eta_{jk}(\Omega,dx) = exp\left[-|\Omega|\, C_x dx \Big/ \left(2\pi\bar{V}_{jk}(z)\right)\right] \tag{18}$$

$$\gamma_{jk}(\Omega,dy,dz) = exp\left[-|\Omega|\sqrt{(C_y dy)^2 + (C_z dz)^2} \Big/ 2\pi\bar{V}_{jk}(z)\right] \tag{19}$$

In the above, dx, dy and dz are $|x_j\text{-}x_k|$, $|y_j\text{-}y_k|$ and $|z_j\text{-}z_k|$, respectively (in m) for two points **j** [coordinate (x_j,y_j,z_j)] and **k** [coordinate (x_k,y_k,z_k)]. $\bar{V}_{jk}(z)$ is $0.5\left[\bar{V}(z_i)+\bar{V}(z_j)\right]$ m/s. C_x, C_y and C_z are the decay parameters, which vary with mean wind speed, turbulence intensity, roughness length, separation distance, wind angle and temperature (Peng *et al.* 2018b). However, in the present paper, the values of C_x, C_y and C_z are taken as 6.0, 16.0 and 10.0, respectively, based on Chen and Letchford (2004), Saranyasoontorn *et al.* (2004), Zhang *et al.* (2008), Gur and Ray-Chaudhuri (2014), Hu *et al.* (2019) and Simiu and Yeo (2019). For the simulation of wind field, the original coordinate system (x,y,z) is transformed to the wind flow direction coordinate system (x', y', z') as:

$$\begin{Bmatrix} x' \\ y' \\ z' \end{Bmatrix} = \begin{pmatrix} \cos\phi & \cos(90-\phi) & \cos 90 \\ \cos(90+\phi) & \cos\phi & \cos 90 \\ \cos 90 & \cos 90 & \cos 0 \end{pmatrix} \begin{Bmatrix} x \\ y \\ z \end{Bmatrix} \tag{20}$$

where, ϕ is the wind incidence angle. The spectral density matrix (SDM), $S^o(\Omega)$ can be expressed as (Popescu *et al.* 1998):

$$\mathbf{S}^o(\Omega) = \begin{bmatrix} S_{11}^o(\Omega) & S_{12}^o(\Omega) & S_{13}^o(\Omega) & \cdots S_{1m}^o(\Omega) \\ S_{21}^o(\Omega) & S_{21}^o(\Omega) & S_{31}^o(\Omega) & \cdots S_{2m}^o(\Omega) \\ \vdots & \vdots & \vdots & \ddots \quad \vdots \\ S_{m1}^o(\Omega) & S_{m2}^o(\Omega) & S_{m3}^o(\Omega) & \cdots S_{mm}^o(\Omega) \end{bmatrix} \tag{21}$$

The diagonal elements of SDM, i.e. S_{jj}^{o} are the PSDF which are real and non-negative functions of Ω. The off-diagonal terms of SDM, i.e. S_{jk}^{o} are the cross-spectral density functions which are complex functions of Ω. The elements of SDM can be taken as (Chen and Letchford 2004):

$$S_{jj}^{o} = S_j(\Omega),\ \forall j \in m,\ j = k;\ \text{and} \quad S_{jk}^{o} = \sqrt{S_j(\Omega)S_k(\Omega)}\eta_{jk}\gamma_{jk},\ \forall j \in m, \forall k \in m, j \neq k \tag{22}$$

In the above, S_j and S_k are the PSDF at j^{th} and k^{th} points, respectively. As the SDM is a Hermitian one, it can be factorized into the upper and lower triangular matrices by Cholesky's method as follows:

$$\mathbf{S}^o(\Omega) = \mathbf{H}(\Omega)\mathbf{H}^{*\mathrm{T}}(\Omega) \tag{23}$$

where, $\mathbf{H}(\Omega)$ is a lower triangular matrix and $\psi_{ij}(\Omega) = tan^{-1}\left(\mathrm{Im}[\mathbf{H}_{ij}(\Omega)]/R_e[\mathbf{H}_{ij}(\Omega)]\right)$.

Finally, $\mathrm{v}(t)$ can be simulated by using the Fast Fourier Transform (FFT) algorithm as (Chen and Zhang 2009):

$$v_i^{(p)}(r\Delta t) = \mathrm{Re}\left\{\sum_{q=1}^{j}\sum_{l=0}^{M-1} B_{jql} exp\left[(ilr\left(\frac{2\pi}{M}\right)\right]\right\} \quad \forall j \in m, \forall p \in M\text{-}1 \tag{24}$$

where, $B_{jql} = 2\left|\mathbf{H}_{jq}(l\Delta\Omega)\right|\sqrt{\Delta\Omega}\, exp\left[-i\psi_{jq}(l\Delta\Omega)\right]exp\left[i\varpi_{ql}^{(i)}\right]$; with $\Delta\Omega = \Omega_u/N$, $\Delta t = 2\pi/M\Delta\Omega$, $M = 2N_f$, and ϖ_{ql} is the random phase angle uniformly distributed over 0 to 2π. Ω_u is the uppercut frequency, N_f is the number of frequency divisions. Finally, the time-history for $F_D(z,t)$ is obtained by Eq. (16). Since, the geometry of a chimney is symmetrical with respect to the central vertical axis, the effect of wind directionality is not studied here. However, this is an important consideration for other tall structures like towers and buildings and should be considered in wind load generation. In this regard, the articles (Ierimonti *et al.* 2017, Bhandari *et al.* 2018, Cui and Caracoglia 2018) may be referred.

For the across-wind component, effect of vortex shedding is an important source of excitation. Large amplitude vibration may take place in a plane normal to the wind flow direction when the vortex shedding frequency is in resonance with one of the natural frequencies of the chimney. The time-varying vortex shedding force can be expressed as:

$$F_L(z,t) = \frac{1}{2}\rho\left[V(z)\right]^2 C_L(z,t)A_i \tag{25}$$

The stochastic lift force co-efficient, $C_L(z,t)$ is obtained by weighted aptitude wave superposition technique (Lipecki and Flaga 2017) with the PSDF of $C_L(z,t)$ as (Vickery and Basu 1983):

$$S_{C_L}(z,\omega)/\sigma_{C_L}^2(z) = \left\{(1/\omega_0)/2\sqrt{\pi}\beta(z)\right\}exp\left\{-\left[1-\omega/\omega_0\right]^2/\beta^2(z)\right\} \tag{26}$$

where, $\omega_0 = 2\pi f_0$ is the vortex shedding frequency and $f_0 = S_t V(z)/D(z)$. S_t is the Strouhal number, assumed as 0.20 (for $D \times V < 6\mathrm{m}^2/\mathrm{s}$) and 0.25 (for $D \times V \geq 6\mathrm{m}^2/\mathrm{s}$) (IS:875-III 2015). $\beta(z)$ is the band-width parameter of the PSDF assumed as 0.25 (Xu *et al.* 2017). $\sigma_{C_L}(z)$ is the SD of C_L which is assumed as invariant over height and taken as 0.4 (Huang and Chen 2007). $D(z)$ is the outside diameter of the chimney at height z from the ground level. Finally, the along-wind force and across-wind force are combined as:

$$F(z,t) = \sqrt{\left\{F_D(z,t)^2 + F_L(z,t)^2\right\}} \tag{27}$$

More details about evaluation of C_L and combination of $F_D(z,t)$ and $F_L(z,t)$ can be found in Venanzi and Materazzi (2012).

6. Incorporation of temperature effect

In RC chimney, brick liner reduces the temperature difference between outer and inner faces of chimney substantially. However, the remaining temperature difference, that yet prevails among the two surfaces are quite considerable. Let, this temperature difference be ΔT. Figs. 1(a), 1(b) and 1(c) depict the vertical section of chimney showing the thickness (t), temperature gradient along the thickness, and stress variation along the thickness, respectively. It can be derived that the maximum compressive stress in concrete (σ_c^T) and tensile stress in steel (σ_s^T) due to temperature difference ΔT are (Bhavikatti 2014):

$$\sigma_c^T = E_c\Delta T\alpha k,\quad \sigma_s^T = E_s\Delta T\alpha(\varphi - k) \tag{28}$$

In the above, kt is the depth of the neutral axis (Fig. 1(c)), which can be obtained as:

$$k = -mp + \sqrt{(m^2p^2 + 2mp\varphi)} \tag{29}$$

where, p is the area percentage of steel reinforcement and m is the modular ratio=E_s/E_c. The hoop stress induced in the circumferential steel due to ΔT can be written as:

$$\sigma_{sh} = (m\sigma_c')(\varphi' - k')/k' \tag{30}$$

Here φ' is the centroidal distance of horizontal reinforcement from the extreme compressive fibre. $k' = -mp + \sqrt{(m^2p^2 + 2mp\varphi')}$ and $\sigma_c' = k'E_c\alpha\Delta T$.

Thus, the stresses in steel and concrete can be directly determined by the Eqns. (28) - (30) if the reinforcement in the chimney is known. Then, the stresses due to wind and temperature are combined (since, wind and temperature are mutually exclusive events) to obtain critical limit states for stress in steel and concrete. Now, to consider the effect of

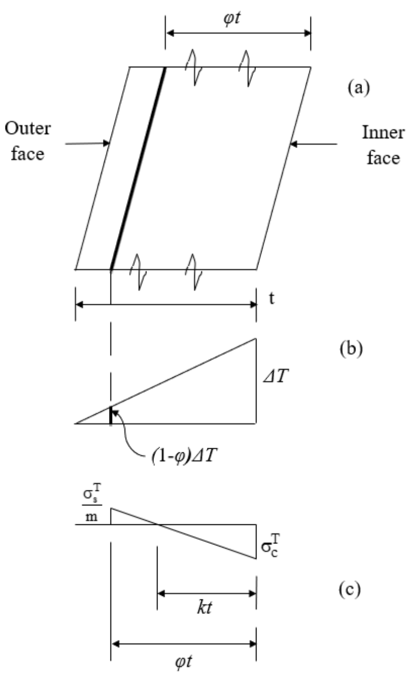

Fig. 1 (a) A sectional elevation of chimney, (b) temperature variation along the thickness, and (c) stress distribution

uncertainty, DRSM based wind fragility procedure is accomplished. This is detailed in the next section.

7. Implementation of the DRSM based WFA

The implementation procedure is described below by means of a flow chart in Fig. 2. At first, the uncertain parameters are selected. Thereafter, their mean, SD and statistical distribution are decided based on the existing literature. Accordingly, the design matrix with $\Re$ design points ($\Re$=20 here) is constructed following Latin Hypercube Sampling (LHS) technique (McKay *et al.* 2000). Then, at each DOE points, l artificial stochastic wind force time-histories are generated (l=10 here). The wind force is computed following Eq. (27). Linear time-history analysis of the finite element model of the chimney is performed at all the DOE points and for each of the l artificially generated wind force time-histories. In the present study, $\overline{V}$ is varied from 10 m/s to 70 m/s at an interval of 10 m/s. Now, for each $\overline{V}$, a bin of l stochastic wind force time-histories is generated. Thus, the time-history analysis is executed for $\Re$ (wind speeds) × l (artificial wind force time-history) i.e. $\Re \times l$ times (=200 in the present case). For each set up of $\overline{V}$, the mean and SD of maximum response (maximum stresses here) are stored for construction of response surfaces. Parallelly, for different ΔT as per DOE, the maximum stress in steel and concrete are calculated and combined with wind effect to obtain the critical limit state of stress. Finally, two response surfaces, one for the mean response, and another for the SD of response are generated for subsequent WFA.

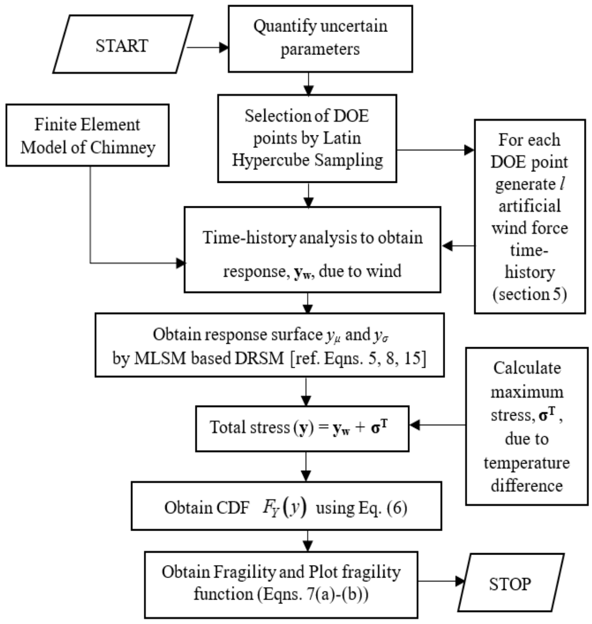

Fig. 2 Implementation of the WFA in the DRSM framework

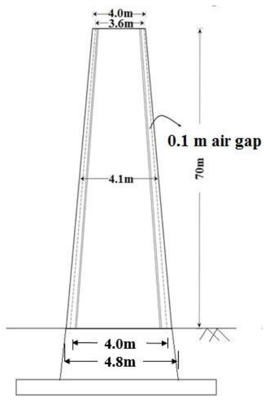

Fig. 3 Sectional elevation of the RC chimney

The key concept of the DRSM are i) the generation of a number of wind force time-history for each set up of $\overline{V}$ to capture record-to-record variation of wind speed, and ii) construction of two response surfaces, one for mean and another for SD of response for accomplishment of WFA as defined in Eqs. (6) and (7(a) - 7(b)). Thereafter, wind fragility of RC chimney for different set up of ΔT and $\overline{V}$ is computed using the developed response surfaces. Once, the dual response surfaces are generated, the WFA can be accomplished without applying direct MCS (see Eqs. 7(a) - 7(b)). Thus, a substantial amount of computational time is expected to be saved by the proposed approach.

8. Numerical study

The proposed WFA of RC chimney is elucidated by considering a 70 m high RC chimney (Fig. 3). The chimney structure is considered to be fixed at the bottom and the top is free. The outside diameter of the chimney is 4.8 m at the base and is uniformly tapered to 4 m at the top. The

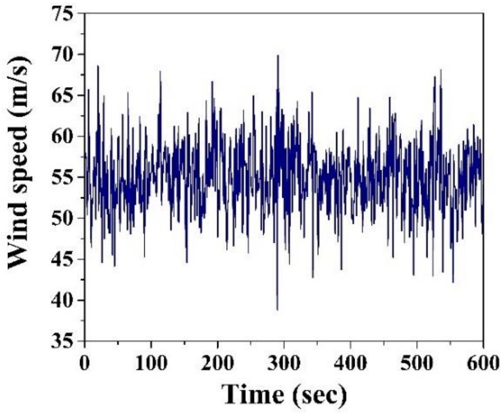

Fig. 4 Wind speed time-history at 30 m level of the chimney for $\bar{V}$ = 50 m/s

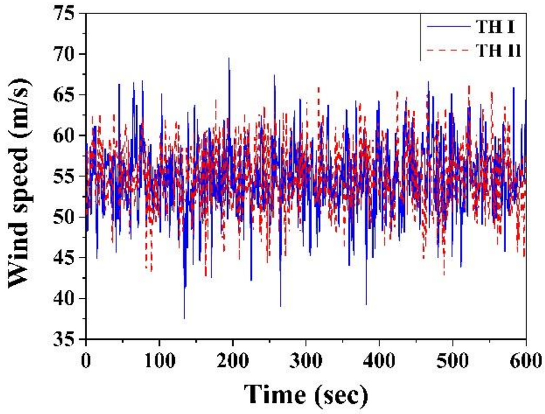

Fig. 6 Two typical wind speed time-histories showing variations for $\bar{V}$ =50 m/s

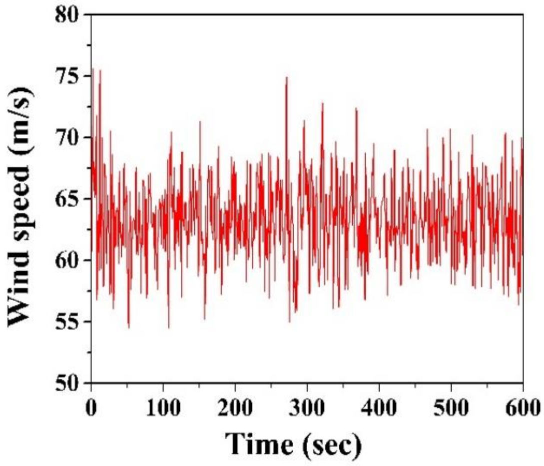

Fig. 5 Wind speed time-history at 70 m level of the chimney for $\bar{V}$ = 50 m/s

thickness of the chimney is 400 mm at the base which is uniformly reduced to 200 mm at top. A deterministic design yields 1% vertical reinforcement and 10 mm bars @ 200 c/c as hoop reinforcement (Bhavikatti 2014). The thickness of the brick lining and air gap both are 100 mm. M25 grade concrete and Fe500 grade steel are adopted. Four temperature differences are considered, viz. 50℃, 100℃, 150℃ and 200℃. Coefficient of thermal expansion is taken as 11×10^{-6}/℃. The chimney has been considered to be uniformly tapered circular in cross-section and modelled with shell elements in FEA software SAP2000.

The wind speed time-histories are generated by using the wind field model as detailed in section 5. Wind speed is varied from 10 m/s to 70 m/s at an interval of 10 m/s and a set of artificially generated wind speed time-histories are obtained at each wind speed. It can be noted that though $\bar{V}$ rarely exceeds 50 m/s, still such a wide range of $\bar{V}$ is considered to yield complete wind fragility curves. Wind speed time-histories are generated at fourteen nodes along the height spaced at 5 m c/c. Two typical along-wind wind speed time-histories obtained for mean wind speed 50 m/s at 30 m and 70 m level of the chimney are shown in Figs. 4 and 5, respectively. The root mean squares dispersion value about the mean for these two time-histories are 3.43 m/s and 4.74 m/s, respectively. The associated average dispersions are 10.08% and 22.85%, respectively. For a particular realization of $\bar{V}$ (50 m/s), two wind speed signatures are plotted in Fig. 6 (TH I and TH II) to reflect the variability in the wind load. It is interesting to observe that the wind speed signatures significantly vary even for the same realization of $\bar{V}$ and other load-related parameters. The average dispersion value of wind speed about the mean is 8.47% and 10.05% for TH I and TH II, respectively. This figure indicates the necessity of applying DRSM in order to capture this record-to-record variation of wind speed.

A comparative study is carried out with different available Indian Standards (IS) relevant to chimney design. The maximum wind speed variation is plotted in Fig. 7 for varying height of the chimney by i) IS 875(III) (1987) (with gust), ii) IS 4988-I (2015) (with gust), iii) IS 875(III) (2015) (with gust), and iv) IS 875(III) (2015) (without gust). IS 4988-I (2015) is a specific code for chimney design; whereas, IS 875 (III) (2015) is a general code for any structure in India. IS 875(III) (1987) is the most conservative approach when gust is considered. In the present study, the ratio of minimum lateral dimension to wall thickness is much lesser than 100 (IS:875-III 2015). Hence, the ovalling effect is not considered. In Fig. 7, the present stochastic wind field approach of wind pressure distribution is not considered. This is because the pressure by the stochastic wind field approach is temporally varying and stochastic in nature unlike the other pressure calculation methods of Fig. 7. Moreover, as per the coherence theory, the maximum wind pressure at all the stories will not be attained simultaneously. Thus, in order to check the compatibility of the time-histories of wind pressure with other methods presented in Fig. 7, the maximum horizontal deflection is compared in Table 1. It may be observed from Table 1 that the stochastic wind field approach yields more deflection than IS 4998-I (2015), but is less than the most conservative IS 875(III) (1987) approach. It is important to

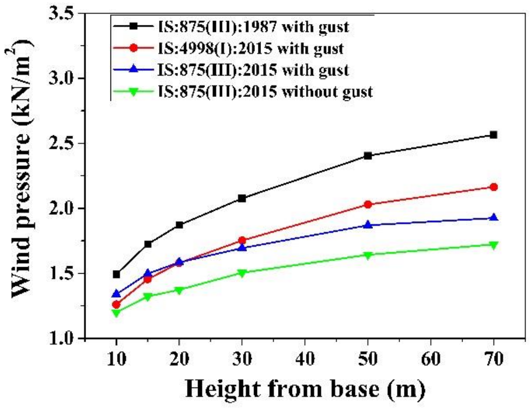

Fig. 7 Wind pressure variation with respect to the height of the chimney

Table 1 Maximum deflection by various wind estimation approach

Approach	IS: 4998-I (2015)	IS:875-III (1987) (with gust)	Stochastic wind field
Maximum top deflection	63.75 mm	86.9 mm	74.8 mm

note that by the stochastic wind field approach, at first, ten wind force time-history sets are simulated using Eq. (27) to consider record-to-record variation of wind speed. Each set comprises of fourteen wind force time-histories for fourteen equidistant levels of the chimney along the height. $\bar{V}$ is taken as 50 m/s. Then, linear time-history analyses are performed using FEA software SAP2000 for each of these wind force sets. The timely-maximum value of lateral deflections is extracted for each level of the chimney for all these wind force time-histories, which yield ten timely-maximum lateral deflection profiles over the height of the chimney for each of the ten sets of wind force. Finally, the mean deflection profile is found out by averaging these ten deflection profiles, the maximum of which (obtained at top node of the chimney) is presented in Table 1. The stochastic wind field being more detailed and realistic approach is adopted in the present study for the WFA.

The behaviour of the chimney is found to be well within the elastic limit under the stochastic wind field. The maximum value of the top deflection observed is 74.8 mm and the allowable elastic limit of deflection of the RC chimney is H_s/500 (=140 mm) (IS:4998-I 2015), where H_s is the total height of the structure (H_s=70 m considered in this numerical study). Hence, a linear time-history analysis has been performed in SAP2000. Also, the material is considered to be homogeneous and isotropic for linear dynamic analysis. Geometric and material non-linearities are neglected.

It can be further noted here that a more general way to treat effect of temperature is to apply a non-linear dynamic analysis of the structure incorporating the effect of cracking, stiffness degradation and tension stiffening. In this regard, Hognestad's model (Hognestad 1951) or EN 1992-1-2 (2004) may be referred. However, in the present study, linear dynamic analysis has been adopted to cater to temperature effects in a simplified way without considering material and geometric non-linearities. This simplified approach is a widely used design practice in India (Manohar 1985, Bhavikatti 2014).

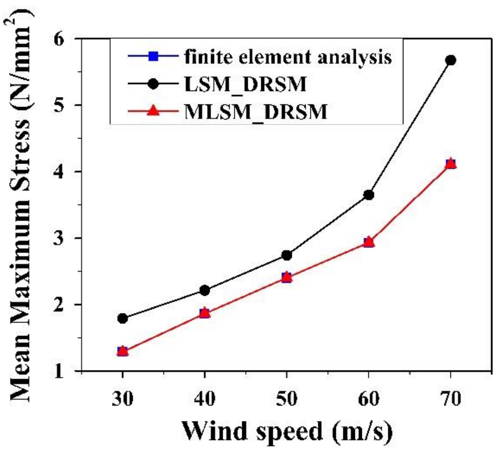

Fig. 8 Validation of the RSM

Table 2 Random Parameters considered in fragility analysis

Parameters	Mean	COV (%)	PDF	Reference
C_D	0.9	10	normal	Le and Caracoglia (2020)
γ_c	25 kN/m^3	10	normal	Masoomi and van de Lindt (2016)
γ_b	20 kN/m^3	10	normal	Masoomi and van de Lindt (2016)
m	13	10	normal	Low and Hao (2001)
$\bar{V}$	varies	30	extreme value type I	Morgan *et al.* (2011)
α	11x10^{-6}/°C	10	normal	-
E_s	2.1x10^8 kN/m^2	10	normal	Masoomi and van de Lindt (2016)
ΔT	50°C-200°C	30	lognormal	-

The response surfaces for the mean and SD of maximum stress under combined wind and temperature effect is obtained by the DRSM. Validation of the actual finite element result of mean maximum stress in concrete with respect to DRSM predicted value is shown in Fig. 8. As discussed, MLSM based RSM (Bhandari *et al.* 2018) has been adopted in the present study in place of conventional LSM based RSM. It may be observed that the MLSM based RSM captures the trend of actual finite element results quite satisfactorily than the conventional LSM based RSM. Hence, the MLSM is applied here to work out the rest of the WFA results. The coefficient of determination value (R^2) (Wright 1921) and root mean square error (RMSE) (Barnston 1992) by the MLSM based RSM are 0.95 and 0.0053, respectively, whereas for LSM based RSM those are 0.83 and 0.000413, respectively which attests the

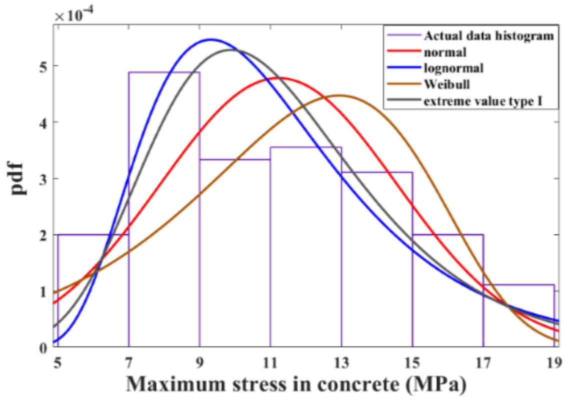

Fig. 9 A typical goodness of fit test

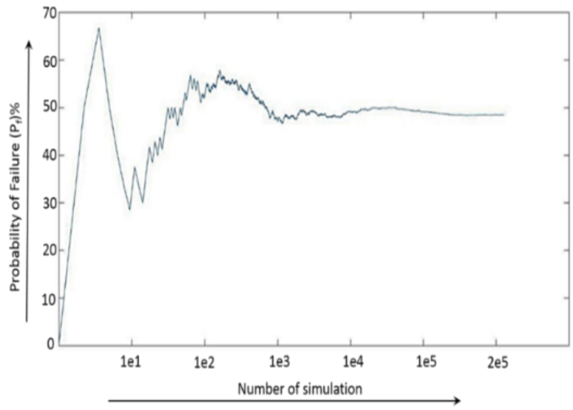

Fig. 10 The convergence of the MCS

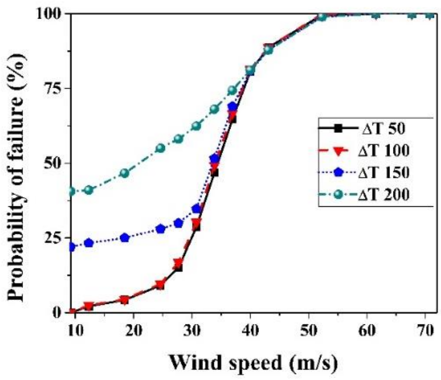

Fig. 11 Wind fragility of RC chimney by conventional single-level RSM

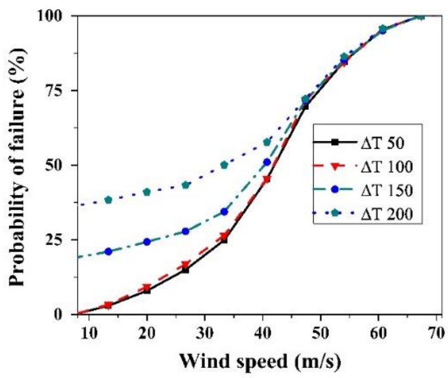

Fig. 12 Wind fragility of RC chimney by the DRSM

accuracy of the MLSM based RSM approximation. The WFA is accomplished using LHS incorporating temperature effect and the uncertainty in the system parameters. The regressors those have been considered to construct response surfaces are:

- Drag coefficient (C_D)
- Wind speed ($\bar{V}$)
- Unit weight of concrete (γ_c)
- Coefficient of thermal expansion (α)
- Unit weight of brick lining (γ_b)
- Modulus of elasticity of steel (E_s)
- Modular ratio (m)
- Temperature difference (ΔT)

The statistical properties of these regressors are presented in Table 2.

To ascertain CDF of the distribution of stresses, a goodness of fit test has been performed. Fig. 9 shows the frequency diagram for maximum stress in concrete. It can be observed that extreme value type I fits best with the statistical trend of actual maximum stress in concrete obtained by FEA. This inference is further validated by a K-S test (Massey 1951). The p-value statistics obtained for the normal, lognormal, Weibull and extreme value type I distributions are 0.11146, 0.84096, 0.57489 and 0.88529, respectively. Since, the extreme value type I distribution yields the highest p-value among these distributions, it can be concluded that the response conforms to the extreme value type I distribution more appropriately. For WFA the limit states of failure considered are: i) maximum stresses in concrete in chimney due to combined effect of self-weight, wind and temperature, ii) associated maximum stress in vertical reinforcement, and iii) hoop stress in horizontal reinforcement. The allowable limits are 8.5 MPa, 230 MPa and 230 MPa, respectively. The fragility is evaluated assuming response distributed as extreme value type I (see Fig. 9). Accordingly, Eq. (7) is used to evaluate the fragility. The MCS is no longer required by the proposed DRSM based approach once the dual response surfaces are generated. However, to validate the efficiency of the proposed approach the WFA is also carried out by the direct MCS approach. The direct MCS converges at 2600 number of simulations. The WFA has been also executed by conventional single-level RSM, wherein the MCS is applied over a general response surface of maximum stress. This approach does not take into account the record-to-record variation of wind speed time-histories. The MCS based single level RSM converges at 6000 simulations. A typical convergence study is presented in Fig. 10.

The fragility curves are shown through Figs. 11-14. Figs. 11 and 12 presents the fragility curves by the conventional single-level RSM and the proposed DRSM, respectively. The fragility curves are presented in terms of probability of failure (P_f) of the chimney for varying wind speed and temperature difference (in °C). It may be noted that at smaller wind speed both the approaches produce analogous results. For example, when $\bar{V}$ =25 m/s and ΔT=100°C, P_f values are 11% and 15% by the single-level RSM and DRSM, respectively. P_f=43% and 40% by the

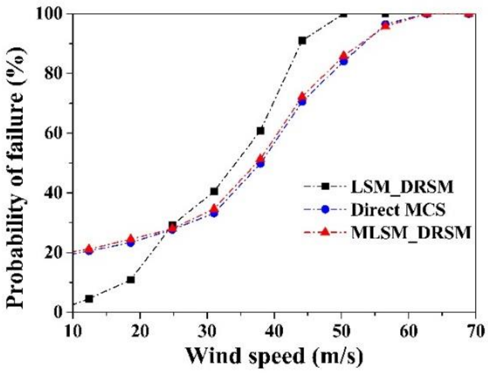

Fig. 13 Comparison of fragility curves for varying wind speed at ΔT=150°C

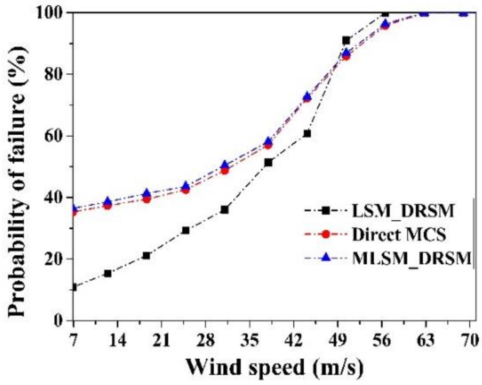

Fig. 14 Comparison of fragility curves for varying wind speed at ΔT=200°C

single-level RSM and DRSM, respectively, when $\bar{V}$ is 18 m/s and ΔT=200°C. However, there is a significant difference between the fragility curves by conventional single-level RSM and the proposed DRSM for higher wind speed values. For example, when $\bar{V}$ is 48 m/s and ΔT=100°C, the single level RSM predicts P_f =86%, whereas, the DRSM predicts P_f= 63%. At $\bar{V}$ =54 m/s, the single level RSM predicts P_f =98%, whereas, the DRSM yields P_f=85%. It can be noted from both of these figures that when $\bar{V}$ = 45 m/s or more, wind governs the design. In such a case, P_f is almost the same for all values of ΔT. It can be observed from these figures that the conventional single-level RSM predicts the values of P_f in the higher side than the DRSM. This may be due to the fact that the single-level RSM considers one typical wind speed time-history for each $\bar{V}$; whereas, in the DRSM a suite of load time-history records corresponding to particular wind speed is considered. In the present case, the single-level RSM is biased towards the higher prediction of risk, but the reverse may also happen. In fact, as the single-level approach does not consider the record-to-record variation of wind speed time-histories, the results may be biased towards the lower or higher side (as in the present case) than the actual. It may be further observed that over ΔT=150°C, the temperature

Table 3 Computational efficiency by the proposed DRSM based fragility analysis procedure

Approach	Direct MCS	MLSM_DRSM	LSM_DRSM
Number of FEA run	2600	200	160
Computational time requirement	847 hours	35 hours	28 hours

stress is so pronounced that P_f is very high even at $\bar{V}$ =35 m/s. At low wind speed ($\bar{V}$ <30 m/s), say around 20 m/s, the temperature difference of 100°C and 150°C yield P_f of 10.5% and 24%, respectively. However, below 100°C, the wind effect is more pronounced than the temperature effect. Although the deterministic design by IS code method (IS:4998-I 2015) is observed to be safe, Fig. 12 shows 21% probability of failure at $\bar{V}$ = 33 m/s and ΔT=50°C.

The probability of failure is plotted for varying $\bar{V}$ with ΔT=150°C and 200°C in Figs. 13 and 14, respectively. The results by the LSM based DRSM, the most accurate direct MCS approach and the proposed MLSM based DRSM approach are also shown in the same figure. The proposed MLSM based DRSM conforms well to the most accurate direct MCS approach endorsing the accuracy of the proposed approach. On the other hand, the conventional LSM predictions significantly deviate from the most accurate direct MCS approach indicating inaccurate prediction by the LSM.

The computational efficiency by the proposed DRSM based WFA is indicated in terms of the number of FEA runs in Table 3. The total computational time required by the three approaches is shown in the same table. A processor with 8 GB RAM and 3.7 GHz clock speed has been used to carry out the fragility analysis. The computational time shown here is inclusive of construction of DOE, generation of metamodel and subsequent fragility evaluations. Table 3 clearly establishes the computational viability of the proposed approach.

The proposed DRSM based WFA approach is efficient for probability of failure more than 10^{-3}. However, for estimating very low probability of failure, techniques like Importance sampling (Denny 2001), kriging (Rasmussen and Williams 2006), polynomial-chaos expansions (Chakraborty and Chowdhury 2017), support vector machines (Gunn 1998), and ensemble of suitable metamodels (Acar and Rais-Rohani 2009) may be explored, which is under consideration at this stage.

9. Conclusions

Wind fragility analysis of an RC chimney is presented incorporating temperature effects. The stochastic artificial wind force time-histories are generated by SRM using Kaimal's PSDF. The limit states of failure composed of exceeding maximum stresses in steel and concrete, which is obtained by a linear time-history analysis of the finite element model of the chimney. The implicit limit state function for the failure of the chimney is approximated by

DRSM framework. The proposed scheme of WFA using DRSM considers the record-to-record variation of wind speed time-histories and provides a more rational basis for WFA than the conventional single-level RSM. Based on the numerical study following conclusions can be summarized:

• The WFA disregarding temperature effects will provide unsafe predictions. It has been observed that over temperature difference of 150°C, the temperature stress is so pronounced that the probability of failure is very high even at low wind speed. However, below 100°C, wind governs the design. It has been further observed that the deterministic design by IS code method is safe at a wind speed of 33 m/s, whereas the proposed method yields 13% probability of failure at that wind speed.

• The results show that the DRSM captures the trend of actual FEA quite satisfactorily. There is a significant deviation in fragility curves between conventional single-level RSM and the proposed DRSM approach of WFA, particularly in higher wind speeds (more than 33 m/s). In the present case, the single-level RSM yields higher risk values than the DRSM. This is because the WFA by conventional single-level RSM considers only one sample of wind speed time-history, which may be inadequate for accurate risk prediction. On the other hand, sufficient wind speed time-history records are taken in DRSM which captures the temporal variation of wind speed in a more detailed way (such as computing the mean, SD and CDF of wind speed).

• By the proposed DRSM based WFA approach, once the dual response surfaces are generated, MCS is not needed to be performed to calculate fragility. As a result, the present approach requires substantially lesser computational time than the conventional direct MCS based approach.

Among the future scope of work, more accurate modelling of temperature difference may be explored. The temperature difference may be assumed as uncertain-but-bounded type. In the present study, the wind fragility is obtained assuming that the high wind loads (which may even cause resonance at critical wind speeds) and high temperature may occur simultaneously. In fact, for a controlled operation of chimney, the probability of their joint occurrence will be at low value; but, for uncontrolled (or unsupervised) operations, there will be a chance of occurrence of these two extreme events simultaneously. If the two events are mutually exclusive, the total failure probability will be affected. This needs further study using site hazard curves and detailed statistical data. For practical interest, the proposed procedure may be implemented for other height and aspect ratios of the chimney with site specific wind and temperature difference data. The proposed approach being generic in nature, can be explored for steel chimneys as well, but the effect of ovalling must be considered in such cases.

Acknowledgements

The financial support received from the Council of Scientific and Industrial Research (CSIR), Govt. of India (Scheme No. 22(0779)/18/EMR-II dated 02/05/2018) in connection with this work is gratefully acknowledged.

References

Abrous, A., Wamkeue, R. and Berkouk, M.E. (2015), “Modeling and simulation of a wind model using a spectral representation method”, *The Proceedings of the 3rd International Renewable and Sustainable Energy Conference*, Marrakech, Morocco, December.

Acar, E. and Rais-Rohani, M. (2009), “Ensemble of metamodels with optimized weight factors”, *Struct Multidisc Optim*, **37**(3), 279–294. https://doi.org/10.1007/s00158-008-0230-y.

Ambrosini, R.D., Riera, J.D. and Danesi, R.F. (2002), “Analysis of structures subjected to random wind loading by simulation in the frequency domain”, *Probabilist Eng Mech*, **17**(3), 233-239. https://doi.org/10.1016/S0266-8920(02)00008-5.

Barnston, A.G. (1992), “Correspondence among the Correlation, RMSE, and Heidke Forecast Verification Measures; Refinement of the Heidke Score”, *Weather Forecast*, **7**(4), 699-709. https://doi.org/10.1175/15200434(1992)007<0699:CATCRA>2.0.CO;2.

Benowitz, B.A. and Deodatis, G. (2015), “Simulation of wind velocities on long span structures: A novel stochastic wave based model”, *J Wind Eng Ind Aerodyn*, **147**, 154-163. https://doi.org/10.1016/j.jweia.2015.10.004.

Bhandari, A., Datta, G. and Bhattacharjya, S. (2018), “Efficient wind fragility analysis of RC high rise building through metamodeling”, *Wind Struct*, **27**(3), 199-211. https://doi.org/10.12989/was.2018.27.3.199.

Bhattacharjya, S. and Chakraborty, S. (2018), “An improved robust multi-objective optimization of structure with random parameters”, *Adv Struct Eng*, **21**(11), 1597-1607. https://doi.org/10.1177/1369433217752626.

Bhattacharjya, S., Sarkar, M., Datta, G. and Ghosh, S.K. (2019), “Efficient Robust Design Optimization of a Stacker–Reclaimer Structure Under Uncertainty”, *Intl. J. Reliab., Quality Safety Eng.*, **26**(2), 1950009. https://doi.org/10.1142/S0218539319500098.

Bhavikatti, S.S. (2014), “Advanced RCC Design”, New Age Publications, New Delhi, India.

Bru, D., Ivorra, S. and Baeza, F.J. (2017), “Seismic behavior of a masonry chimney retrofitted with composite materials: a preliminary approach”, *Int J of Safety Security Eng*, **7**(4), 486-497. https://doi.org/10.2495/SAFE-V7-N4-486-497.

Chakraborty, S. and Chowdhury, R. (2017), “Hybrid Framework for the Estimation of Rare Failure Event Probability”, *J Eng Mech*, **143**(5), 04017010. https://doi.org/10.1061/(ASCE)EM.1943-7889.0001223.

Chen, J. and Zhang, X. (2009), “An empirical joint probability density function of wind speed and direction”, *Proceedings of The Seventh Asia-Pacific Conference on Wind Engineering*, Taipei, Taiwan, November.

Chen, J., Chen, Y., Peng, Y., Zhu, S., Beer, M. and Comerford, L. (2019), “Stochastic harmonic function based wind field simulation and wind-induced reliability of super high-rise buildings”, *Mech. Syst. Sig. Pr.*, **133**, 106264. https://doi.org/10.1016/j.ymssp.2019.106264.

Chen, J., Zeng, X. and Peng, Y. (2017), “Probabilistic analysis of wind-induced vibration mitigation of structures by fluid viscous dampers” *J Sound Vib*, **409**, 287-305. https://doi.org/10.1016/j.jsv.2017.07.051.

Chen, L. and Letchford, C.W. (2004), “A deterministic–stochastic hybrid model of downbursts and its impact on a cantilevered structure", *Eng Struct*, **26**(5), 619-629. https://doi.org/10.1016/j.engstruct.2003.12.009.

Chen, X. and Kareem, A. (2004), "Equivalent static wind loads on buildings: new Model" *J Struct Eng*, **130**(10), 1425-1435. https://doi.org/10.1061/(ASCE)0733-9445(2004)130:10(1425).

Cui, W. and Caracoglia, L. (2018), "A unified framework for performance-based wind engineering of tall buildings in hurricane-prone regions based on lifetime intervention-cost estimation", *Struct. Saf*, **73**, 75-86. https://doi.org/10.1016/j.strusafe.2018.02.003.

Denny, M. (2001), "Introduction to importance sampling in rare-event simulations", *Eur J Phys*, **22**(4), 403–11. https://doi.org/10.1088/0143-0807/22/4/315.

Deodatis, G. and Micaletti, R.C. (2001), "Simulation of highly skewed non-Gaussian stochastic processes" *J. Eng. Mech.*, **127**(12), 1284-1295. https://doi.org/10.1061/(ASCE)0733-9399(2001)127:12(1284).

Di Paola, M. (1998), "Digital simulation of wind field velocity" *J Wind Eng. Indus. Aerod.*, **74-76**, 91-109. https://doi.org/10.1016/S0167-6105(98)00008-7.

EN 1992-1-2, Eurocode 2 (2004), Design of Concrete Structures. Part 1.2: General Rules-Structural Fire Design, Commission of the European Communities, Brussels, Belgium.

Feng, R., Wang, X., Yuan, W. and Yu, J. (2018), "Impact of seismic excitation direction on the fragility analysis of horizontally curved concrete bridges", *B. Earthq. Eng*, **16**(10), 4705–4733. https://doi.org/10.1007/s10518-018-0400-2.

Ghosh, S., Ghosh, S. and Chakraborty, S. (2017b), "Seismic fragility analysis in the probabilistic performance-based earthquake engineering framework: an overview", *Intl. J. Adv. Eng. Sci. Appl. Math.*, https://doi.org/10.1007/s12572-017-0200-y.

Ghosh, S., Ghosh, S. and Chakraborty, S. (2018), "Seismic reliability analysis of reinforced concrete bridge pier using efficient response surface method–based simulation", *Adv. Struct. Eng.*, **21**(15), 2326-2339. https://doi.org/10.1177/1369433218773422.

Ghosh, S., Mitra, S., Ghosh, S. and Chakraborty, S. (2017a), *Seismic Reliability Analysis in the Framework of Metamodelling Based Monte Carlo Simulation*, Modeling and Simulation Techniques in Structural Engineering, eds. Pijush Samui, Subrata Chakraborty and Dookie Kim, 192-208, accessed July 15, 2019.

Giaccu, G.F. and Caracoglia, L. (2018), "Wind-load fragility analysis of monopole towers by layered stochastic approximation-Monte-Carlo method", *Eng. Struct.*, **174**, 462-477. https://doi.org/10.1016/j.engstruct.2018.07.081.

Goswami, S., Ghosh, S. and Chakraborty, S. (2016), "Reliability analysis of structures by iterative improved response surface method", *Struct. Saf.*, **60**, 56-66. https://doi.org/10.1016/j.strusafe.2016.02.002.

Gunn, S. (1998), "Support vector machines for classification and regression" Rep. No. ISIS-1-98; Department of Electronics and Computer Science, Univ. of Southampton, Southampton, U.K.

Gur, S. and Ray-Chaudhuri, S. (2014), "Vulnerability assessment of container cranes under stochastic wind loading", *Struct. Infrastruct. E.*, **10**(12), 1511-1530. https://doi.org/10.1080/15732479.2013.834943.

Harris, R.I. (1990), "Some further thoughts on the spectrum of gustiness in strong winds", *J. Wind Eng. Indus. Aerod.*, **33**(3), 461-477. https://doi.org/10.1016/0167-6105(90)90001-S.

Hognestad, E. (1951), *A Study of Combined Bending and Axial Load in Reinforced Concrete Members*, University of Illinois at Urbana Champaign, College of Engineering, Engineering Experiment Station, Bulletin Series No. 399.

Hu, P., Han, Y., Cai, C.S., Cheng, W. and Lin, W. (2019), "New analytical models for power spectral density and coherence function of wind turbulence relative to a moving vehicle under crosswinds", *J. Wind Eng. Indus. Aerod.*, **188**, 384-396. https://doi.org/10.1016/j.jweia.2019.02.005.

Huang, G. and Chen, X. (2007), "Wind load effects and equivalent static wind loads of tall buildings based on synchronous pressure measurements", *Eng. Struct.*, **29**(10), 2641-2653. https://doi.org/10.1016/j.engstruct.2007.01.011.

Ierimonti, L., Caracoglia, L., Venanzi, I. and Materazzi, A.L. (2017), "Investigation on life-cycle damage cost of wind-excited tall buildings considering directionality effects", *J Wind Eng. Indus. Aerod.*, **171**, 207-218. https://doi.org/10.1016/j.jweia.2017.09.020.

IS 456 (2000), "Plain and reinforced concrete - Code of practice", Bureau of Indian Standards, India.

IS 4998-I (2015), "Criteria for Design of Reinforced Concrete Chimneys, Part-I, Assessment of Loads", Bureau of Indian Standards, India.

IS 875 (III) (1987), "Code of Practice for Design Loads (Other Than Earthquake) For Buildings and Structures Part 3 Wind Loads", Bureau of Indian Standards, India.

IS 875 (III) (2015), "Design Loads (Other than Earthquake) for Buildings and Structures - Code of Practice Part 3 Wind Loads (Third Revision)", Bureau of Indian Standards, India.

Kaimal, J.C., Wyngaard, J.C., Izumi, Y. and Cote, O.R. (1972), "Spectral characteristics of surface-layer turbulence", *Q. J. Roy. Meteorol. Soc.*, **98**(417), 563-589. https://doi.org/10.1002/qj.49709841707.

Karaca, Z. and Turkeli, E. (2014), "The slenderness effect on wind response of industrial reinforced concrete chimneys", *Wind Struct.*, **18**(3), 281-294. https://doi.org/10.12989/was.2014.18.3.281.

Kareem, A. (1988), "Effect of parametric uncertainties on wind excited structural response", *J. Wind Eng. Indus. Aerod.*, **30**(1-3), 233-241. https://doi.org/10.1016/0167-6105(88)90088-8.

Kareem, A. (1990), "Reliability analysis of wind-sensitive structures", *J. Wind Eng. Indus. Aerod.*, **33**(3), 495-514. https://doi.org/10.1016/0167-6105(90)90004-V.

Kareem, A. and Hseih, J. (1986), "Reliability analysis of concrete chimneys under wind loading", *J. Wind Eng. Indus. Aerod.*, **25**(1), 93-112. https://doi.org/10.1016/0167-6105(86)90106-6.

Le, V. and Caracoglia, L. (2020), "Life-cycle cost analysis of a point-like structure subjected to tornadic wind loads", *J. Struct. Eng.*, **146**(2), 04019194. https://doi.org/10.1061/(ASCE)ST.1943-541X.0002480.

Lee, K.H. and Rosowsky, D.V. (2006), "Fragility curves for woodframe structures subjected to lateral wind loads", *Wind Struct.*, **9**(3), 217-230. https://doi.org/10.12989/was.2006.9.3.217.

Li, Y., Liao, H. and Qiang, S. (2004), "Simplifying the simulation of stochastic wind velocity fields for long cable-stayed bridges", *Comput. Struct.*, **82**(20-21), 1591-1598. https://doi.org/10.1016/j.compstruc.2004.05.007.

Liang, S., Yang, W., Song, J., Wang, L. and Hu, G. (2018), "Wind-induced responses of a tall chimney by aeroelastic wind tunnel test using a continuous model", *Eng. Struct.*, **176**, 871-880. https://doi.org/10.1016/j.engstruct.2018.09.015.

Lipecki, T. and Flaga, A. (2017), "Application of simulation methods of stochastic processes to vortex excitation", *Arch. Civ. Eng.*, **63**(1), 77-97. https://doi.org/10.1515/ace-2017-0006.

Liu, Z., Liu, Z. and Peng, Y. (2018), "Simulation of multivariate stationary stochastic processes using dimension-reduction representation methods", *J. Sound Vib.*, **418**, 144-162. https://doi.org/10.1016/j.jsv.2017.12.029.

Low, H.Y. and Hao, H. (2001), "Reliability analysis of reinforced concrete slabs under explosive loading", *Struct. Saf.*, **23**(2), 157-178. https://doi.org/10.1016/S0167-4730(01)00011-X.

Manohar, S.N. (1985), "Tall Chimneys", Tata McGraw-Hill Publishing Company Limited, New Delhi, India.

Martinez-Vazquez, P. (2016), "Wind-induced vibrations of structures using design spectra", *Intl. J. Adv. Struct. Eng.*, **8**, 379-389. https://doi.org/10.1007/s40091-016-0139-4.

Masoomi, H. and van de Lindt, J.W. (2016), "Tornado fragility and risk assessment of an archetype masonry school building", *Eng. Struct.*, **128**, 26-43. https://doi.org/10.1016/j.engstruct.2016.09.030.

Massey, F.J. (1951), "The Kolmogorov-Smirnov test for goodness of fit", *J. Am. Stat. Assoc.*, **46**(253), 68-78. https://doi.org/10.1080/01621459.1951.10500769.

McKay, M.D., Beckman, R.J. and Conover, W.J. (2000), "A comparison of three methods for selecting values of input variables in the analysis of output from a computer code", *Technometrics*, **42**(1), 55-61. https://doi.org/10.1080/00401706.2000.10485979.

Morgan, E.C., Matthew, L., Vogel, R.M. and Baise L.G. (2011), "Probability distributions for offshore wind speeds", *Energy Convers. Manage.*, **52**(1), 15-26. https://doi.org/10.1016/j.enconman.2010.06.015.

Myers, R.H., Montgomery, D.C. and Anderson-Cook, C.M. (2016), "Response Surface Methodology: Process and Product in Optimization Using Designed Experiments", John Wiley & Sons, Inc. New York, NY, U.S.A.

Park, S.J., Jang, D., Yook, S.J. and Lee, K.S. (2016), "Optimization of a chimney design for cooling efficiency of a radial heat sink in a LED downlight", *Energy Convers. Manage*, **114**, 180-187. https://doi.org/10.1016/j.enconman.2016.02.024.

Peng, Y., Wang, S. and Li, J. (2018b), "Field measurement and investigation of spatial coherence for near-surface strong winds in Southeast China", *J. Wind Eng. Indus. Aerod.*, **172**, 423-440. https://doi.org/10.1016/j.jweia.2017.11.012.

Peng, Y., Wang, Z. and Ai, X. (2018a), "Wind-induced fragility assessment of urban trees with structural uncertainties", *Wind Struct.*, **26**(1), 45-56. https://doi.org/10.12989/was.2018.26.1.045.

Popescu, R., Deodatis, G. and Prevost, J.H. (1998), "Simulation of homogeneous nonGaussian stochastic vector fields", *Probab. Eng. Mech.*, **13**(1), 1-13. https://doi.org/10.1016/S0266-8920(97)00001-5.

Rasmussen, C.E. and Williams, C.K.I. (2006). *Gaussian processes for machine learning*, MIT Press, Cambridge.

Reuter, I., Voigt, M., Mailach, R., Becker, K.H., Fischersworring-Bunk, A., Schlums, H. and Ivankovic, M. (2017), "Moving least squares metamodels.-hyperparameter, variable reduction and model selection", In: Caspeele, R., Taerwe, L., Proske, D. (eds) 14th International Probabilistic Workshop, Springer, Cham. https://doi.org/10.1007/978-3-319-47886-9_5.

Sancibrian, R., Lombillo, I., Sarabia, E.G., Boffill, Y., Wong, H. and Villegas, L. (2017), "Dynamic identification and condition assessment of an old masonry chimney by using modal testing", *Procedia Eng*, **199**, 3410-3415. https://doi.org/10.1016/j.proeng.2017.09.485.

Saranyasoontorn, K., Manuel, L. and Veers, P.S. (2004), "A comparison of standard coherence models for inflow turbulence with estimates from field measurements" ASME. *J Sol Energy Eng*, **126**(4), 1069-1082. https://doi.org/10.1115/1.1797978

Shinozuka, M. (1971), "Simulation of multivariate and multidimensional random processes" *J. Acoust. Soc. Am.*, **49**(1), 357-368. https://doi.org/10.1121/1.1912338.

Simiu, E. and Scanlan, H.R. (1986), "Wind effects on structure", John Wiley and Sons, New York, NY.

Simiu, E. and Yeo, D.H. (2019), "Wind effects on structure", John Wiley and Sons, New York, N.Y.

Smith, M.A. and Caracoglia, L. (2011), "A Monte Carlo based method for the dynamic fragility analysis of tall buildings under turbulent wind loading", *Eng. Struct*, **33**(2), 410-420. https://doi.org/10.1016/j.engstruct.2010.10.024.

Tabbuso, P., Spence, S.M.J., Palizzolo, L., Pirrotta, A. and Kareem, A. (2016), "An efficient framework for the elasto-plastic reliability assessment of uncertain wind excited systems", *Struct. Saf.*, **58**, 69-78. https://doi.org/10.1016/j.strusafe.2015.09.001.

Taflanidis, A.A. and Cheung, S.H. (2012), "Stochastic sampling using moving least squares response surface methodologies", *Probab. Eng. Mech.*, **28**, 216-224. https://doi.org/10.1016/j.probengmech.2011.07.003.

Venanzi, I. and Materazzi, A.L. (2012), "Acrosswind aeroelastic response of square tall buildings: a semi-analytical approach based of wind tunnel tests on rigid models", *Wind Struct.*, **15**(6), 495-508. https://doi.org/10.12989/was.2012.15.6.495.

Venanzi, I., Materazzi, A.L. and Ierimonti, L. (2015), "Robust and reliable optimization of wind-excited cable-stayed masts", *J. Wind Eng. Ind. Aerodyn.*, **147**, 368-379. https://doi.org/10.1016/j.jweia.2015.07.011.

Vickery, B.J. and Basu, R.I. (1983), "Across-wind vibrations of structures of circular cross-section. Part I. Development of a mathematical model for two-dimensional conditions", *J. Wind Eng. Indus. Aerod.*, **12**(1), 49-73. https://doi.org/10.1016/0167-6105(83)90080-6.

Wright, S. (1921), "Correlation and causation", *J. Agric. Res.*, **20**(7), 557-585.

Xu, J., Spencer, B.F., Lu, X., Chen, X. and Lu, L. (2017), "Optimization of structures subject to stochastic dynamic loading", *Comput. Aided Civil Infrastruct. Eng.*, **32**(8), 657-673. https://doi.org/10.1111/mice.12274.

Zeng, X., Peng, Y. and Chen, J. (2017), "Serviceability-based damping optimization of randomly wind-excited high-rise buildings", *Struct. Des. Tall Spec.*, **26**(11), e1371. https://doi.org/10.1002/tal.1371.

Zhang, L.L., Li, J. and Peng, Y. (2008), "Dynamic response and reliability analysis of tall buildings subject to wind loading", *J. Wind Eng. Indus. Aerod.*, **96**(1), 25-40. https://doi.org/10.1016/j.jweia.2007.03.001.

Zhao, W., Fan, F. and Wang, W. (2017), "Non-linear partial least squares response surface method for structural reliability analysis", *Reliab. Eng. Syst. Safe*, **161**, 69-77. https://doi.org/10.1016/j.ress.2017.01.004.

Zhou, C., Tian, M., Wang, P. and Zhang, X. (2017), "Analysis on structural fragility of a high-rise RC chimney considering ground motion directionality", *J. Hunan Univ.* (*Nat. Sci.*), **44**(11), 11-22. https://doi.org/10.16339/j.cnki.hdxbzkb.2017.11.002.

Zhou, C., Zeng, X., Pan, Q. and Liu, B. (2015), "Seismic fragility assessment of a tall reinforced concrete chimney", *Struct. Des. Tall Spec.*, **24**(6), 440-460. https://doi.org/10.1002/tal.1173.

CC

Appendix

List of Acronyms

CDF	cumulative distribution function	MLSM	moving-least-squares method
COV	coefficient of variation	PDF	probability distribution function
DOE	design of experiment	PSDF	power spectral density function
DRSM	dual response surface method	RC	reinforced concrete
FEA	finite element analyses	RMSE	root mean square error
FFT	Fast Fourier Transform	RSM	response surface method
LHS	Latin Hypercube Sampling	SD	standard deviation
LSM	least-squares method	SDM	spectral density matrix
MCS	Monte Carlo simulation	WFA	wind fragility analysis